nature neuroscience

An evolutionary recent neuroepithelial cell adhesion function of huntingtin implicates ADAM10-Ncadherin

Valentina Lo Sardo[1,7], Chiara Zuccato[1,7], Germano Gaudenzi[2], Barbara Vitali[1], Catarina Ramos[1,6], Marzia Tartari[1], Michael A Myre[3], James A Walker[3], Anna Pistocchi[2], Luciano Conti[1], Marta Valenza[1], Binia Drung[4], Boris Schmidt[4], James Gusella[3], Scott Zeitlin[5], Franco Cotelli[2] & Elena Cattaneo[1]

The Huntington's disease gene product, huntingtin, is indispensable for neural tube formation, but its role is obscure. We studied neurulation in htt-null embryonic stem cells and htt-morpholino zebrafish embryos and found a previously unknown, evolutionarily recent function for this ancient protein. We found that htt was essential for homotypic interactions between neuroepithelial cells; it permitted neurulation and rosette formation by regulating metalloprotease ADAM10 activity and Ncadherin cleavage. This function was embedded in the N terminus of htt and was phenocopied by treatment of htt knockdown zebrafish with an ADAM10 inhibitor. Notably, in htt-null cells, reversion of the rosetteless phenotype occurred only with expression of evolutionarily recent htt heterologues from deuterostome organisms. Conversely, all of the heterologues that we tested, including htt from *Drosophila melanogaster* and *Dictyostelium discoideum*, exhibited anti-apoptotic activity. Thus, anti-apoptosis may have been one of htt's ancestral function(s), but, in deuterostomes, htt evolved to acquire a unique regulatory activity for controlling neural adhesion via ADAM10-Ncadherin, with implications for brain evolution and development.

Huntingtin (htt) is the 3,144 amino acid protein encoded by *Hdh* (also known as *Htt*). *Hdh* contains a polymorphic tri-nucleotide CAG repeat that is translated into polyglutamine amino acid (polyQ) residues in htt. When this polyQ stretch at the 18 amino acid position expands to over 39 residues, Huntington's disease occurs, a fatal, genetically dominant, neurodegenerative disease[1]. The CAG repeats are conserved in deuterostomes, which suggests that they are an ancestral feature that was retained during htt evolution[2]. Consequently, htt is found in *Dictyostelium discoideum*, a lower metazoa at the base of the protostome-deuterostome divergence[3,4]. In *D. discoideum*, however, the protein carries no glutamine at this location and no glutamines are present in protostomes. As evolution progressed, two glutamines appeared in the htt of the sea urchin (*Strongylocentrotus purpuratus*)[2]. Thereafter, glutamines have been maintained in the same position, but have progressively expanded during deuterostome evolution.

In mammals, htt is expressed in the early post-fertilization stages and becomes enriched in the developing and adult brain[5], where it carries out a number of brain-specific activities. It promotes the transcription of neuronal genes, vesicle trafficking and axonal transport[6]. It also acts as an anti-apoptotic protein in brain tissue[7–10] and in cultured neural and peripheral cells[11–13]. During embryogenesis, htt is critical for gastrulation[14–17] and neurogenesis. When htt expression is experimentally reduced to below 50% of wild-type levels, defects in the epiblast are observed[18,19]. In the htt knockdown zebrafish embryo, defects are found in the most anterior regions of the neural plate[20]. Later in development, neuroblasts in the telencephalon must synthesize htt to progress correctly through differentiation[21]. This might depend on a recent finding that htt regulates mitotic spindle orientation in the developing mammalian cortex, an activity that can affect cortical progenitor cell fate decisions[22]. Despite this knowledge, the exact cellular and molecular functions that make htt indispensable for neural tube formation and brain morphogenesis remain largely obscure.

We investigated the function of htt by studying htt-deficient mouse embryonic stem (ES) cells that form neural rosettes, radial arrangements of columnar cells that express many of the proteins found in the neuroepithelium *in vivo*[23,24]. We found that, during neurulation, htt favored homotypic interactions between neuroepithelial cells by inhibiting both the activity of the metalloprotease ADAM10 and Ncadherin cleavage. This also occurred *in vivo*, as defects in neural tube morphogenesis that were observed in htt knockdown zebrafish (*Danio rerio*) embryos could be rescued after treatment with GI254023X, an ADAM10 inhibitor[25].

Finally, we found that this neural cell adhesion function of htt is embedded in its first ~500 amino acids and is unique to late deuterostomes, as htt from a protostome homolog and from more ancient organisms in the deuterostome branch that have a low degree of nervous system centralization could not complement the *rosetteless* phenotype in htt-null ES cells. We conclude that, during deuterostome evolution, particularly after cephalochordate emergence,

[1]Department of Pharmacological Sciences and Centre for Stem Cell Research, Università degli Studi di Milano, Milano, Italy. [2]Department of Biology, Università degli Studi di Milano, Milano, Italy. [3]Center for Human Genetic Research, Massachusetts General Hospital, Boston, Massachusetts, USA. [4]Clemens Schöpf Institute of Chemistry and Biochemistry, Technische Universität Darmstadt, Darmstadt, Germany. [5]Department of Neuroscience, University of Virginia School of Medicine, Charlottesville, Virginia, USA. [6]Present address: Instituto de Medicina Molecular, Av. Prof. Egas Moniz, Lisboa, Portugal. [7]These authors contributed equally to this work. Correspondence should be addressed to E.C. (elena.cattaneo@unimi.it).

Received 14 November 2011; accepted 5 March 2012; published online 1 April 2012; doi:10.1038/nn.3080

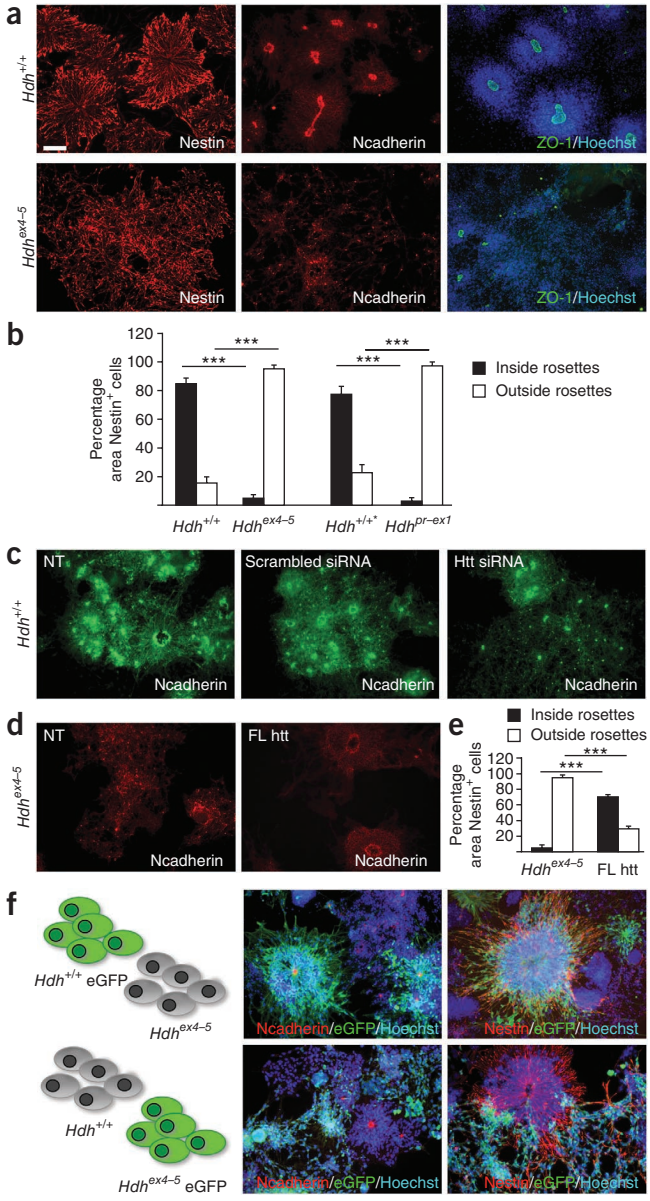

Figure 1 Neural differentiation of htt-null mouse ES cells. (**a**) htt-null ($Hdh^{ex4–5}$)[14] and wild-type ($Hdh^{+/+}$) ES cells were immunostained with Nestin, Ncadherin and ZO-1/Hoechst. (**b**) Quantification of the rosetteless phenotype in htt-null and wild-type cells. Data are the mean ± s.e.m. of five independent experiments for $Hdh^{ex4–5}$ and $Hdh^{+/+}$ cells and from three independent experiments for $Hdh^{pr–ex1}$ and $Hdh^{+/+*}$ cells. ***$P < 0.0001$. $Hdh^{+/+}$ and $Hdh^{+/+*}$ cells are two different batches of wild-type ES cells. (**c**) htt depletion with siRNA in $Hdh^{+/+}$ cells. NT, not transfected with siRNA. (**d**) Expression of mouse full-length htt (FL htt) in $Hdh^{ex4–5}$ cells. NT, not transfected. (**e**) Quantification of neural rosettes after mouse full-length htt expression in $Hdh^{ex4–5}$ cells. Data are the mean ± s.e.m. of three independent experiments. (**f**) Top, $Hdh^{+/+}$ eGFP-labeled cells were co-cultured with an equal amount of unlabeled $Hdh^{ex4–5}$ cells. Bottom, $Hdh^{+/+}$ cells were co-cultured with an equal number of eGFP-labeled $Hdh^{ex4–5}$ cells ($Hdh^{ex4–5}$ eGFP). Co-cultures were immunostained for eGFP, Hoechst and either Ncadherin or Nestin. All immunostaining was conducted on day 8 of neural differentiation. *P* values were determined by two-tailed, unpaired *t* test. Scale bar indicates 75 µm.

htt acquired a cell-adhesion function that is critical for neurulation and that depends on ADAM10 activity.

RESULTS

htt controls interactions between neuroepithelial cells

ES cells that expressed either wild-type htt ($Hdh^{+/+}$ cells) or no htt ($Hdh^{ex4–5}$ cells)[14] were subjected to a monolayer neural differentiation protocol that converts ES cells into neuroepithelial progenitors that resemble those present *in vivo* at the time of neural plate closure and neural tube formation[26]. $Hdh^{+/+}$ cells typically formed neuroepithelial rosettes between days 5 and 7 of differentiation (**Fig. 1a**), which consist of neuroepithelial cells that express the neural stem cell marker Nestin and the apical markers Ncadherin and ZO-1 (ref. 26). In contrast, differentiated $Hdh^{ex4–5}$ cells generated neuroepithelial cells with aberrant spatial organization, and these cultures were nearly devoid of properly formed rosettes (**Fig. 1a** and **Supplementary Videos 1** and **2**). We termed this phenotype rosetteless because these cells never reverted to normal rosettes formation. Furthermore, $Hdh^{ex4–5}$ cells did not display the typical luminal staining of Ncadherin and ZO-1 (**Fig. 1a**), which suggests that the loss of htt leads to defects in neuroepithelial cell polarization during *in vitro* neurulation. Identical results were obtained using a different htt-null ES cell line ($Hdh^{pr–ex1}$)[16] (**Supplementary Fig. 1**). This phenotype did not depend on defects in neural induction, as judged by Sox1 immunoreactivity, which was similar in the two genotypes (**Supplementary Fig. 1**), or on cell density, as increasing amount of $Hdh^{ex4–5}$ cells did not lead to rosettes formation (**Supplementary Fig. 1**). In addition, in control $Hdh^{+/+}$ cultures, the majority (84.4 ± 3.9%) of Nestin$^+$ cells were organized in rosettes; in contrast, in $Hdh^{ex4–5}$ cells, 95.2 ± 1.2% of the Nestin$^+$ cells were dispersed outside of the defective rosette structures on day 8 of monolayer differentiation (**Fig. 1b**). The rare rosette-like formations that were present in knockout cells were smaller in size than $Hdh^{+/+}$ rosettes on day 8 ($Hdh^{ex4–5}$, 80–150 µm; $Hdh^{+/+}$, 300–500 µm). Furthermore, when htt expression was blocked by injecting htt-specific small interfering RNA (siRNA) into $Hdh^{+/+}$ cells 24 h before neural differentiation was initiated (**Supplementary Fig. 2**), we observed a reduction in rosettes number and size on day 8 compared with cells treated with scrambled siRNA (**Fig. 1c**). Finally, expression of exogenous full-length mouse htt from day 0 or acutely at day 2 or 3 (but not later) led to a substantial rescue of the rosetteless phenotype in $Hdh^{ex4–5}$ cells (**Fig. 1d**), as 70 ± 3% of Nestin$^+$ cells were found organized inside the rosettes (**Fig. 1e** and **Supplementary Fig. 3**). These data indicate that htt is required for the organization of neuroepithelial cells into neural rosettes and that the loss of htt alters this process.

To test whether htt's function during rosette formation is cell-autonomous, we established a co-culture system composed of equal amounts of $Hdh^{+/+}$ and $Hdh^{ex4–5}$ ES cells, and modified one of the cell types for stable expression of enhanced green fluorescent protein (eGFP). In a non–cell-autonomous mechanism, we expect that the presence of $Hdh^{+/+}$ cells would induce $Hdh^{ex4–5}$ cells to form rosettes or that $Hdh^{ex4–5}$ cells might be trapped in $Hdh^{+/+}$ rosettes. Instead, neural rosettes were always exclusively composed of $Hdh^{+/+}$ cells (**Fig. 1f** and **Supplementary Video 3**), and $Hdh^{ex4–5}$ cells were unable to form neural rosettes, even in the presence of $Hdh^{+/+}$ cells. We concluded that the ability of htt to promote rosette formation is cell-autonomous.

We next tested the effects of knocking down htt during neural tube morphogenesis in zebrafish by injecting zebrafish embryos with a translation-blocking morpholino oligonucleotide that specifically targeted htt (httMO)[27]. Four categories of embryos, which we termed class 1–4, were generated. Class 1 morphants were similar to control embryos and class 2 morphants showed a reduction of the cephalic region and an attempt of tail curvature that developed into an altered

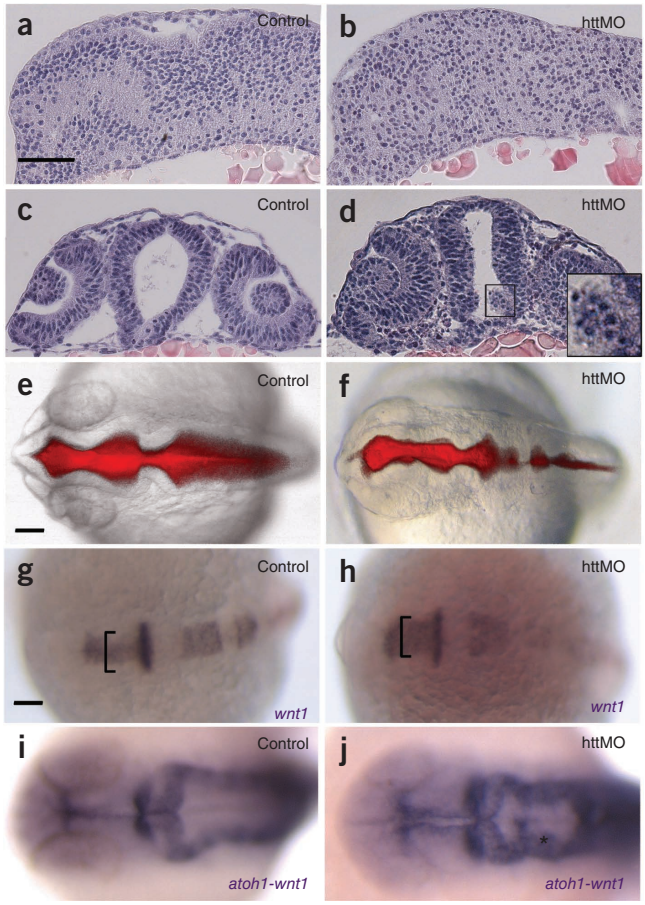

Figure 2 Neural tube impairment in htt loss-of-function zebrafish embryos. (**a**,**b**) Sagittal sections of control and htt knockdown zebrafish embryos (httMO) at somite stage 10 (14 hpf) stained with haematoxylin and eosin. (**c**,**d**) Cross-sections of the neural tube in control and httMO embryos at 24 hpf. (**e**,**f**) Control and httMO brain ventricles injected with rhodamine and dextran at 24 hpf. One representative section of ~100 morphant and control embryos subjected to four independent httMO injections is shown. (**g**,**h**) *wnt1* whole-mount *in situ* hybridization at somite stage 7–8, dorsal view with anterior to the left. The brackets indicate the expansion of the midbrain *wnt1* expression domain in httMO in comparison with control embryos. (**i**,**j**) *wnt1* and *atoh1* double whole-mount *in situ* hybridization at 24 hpf, dorsal view with anterior to the left. Midbrain roofplate and rombomeric boundaries of httMO embryos were disorganized and fused anteriorly in comparison with controls. Asterisk indicates the disorganization of the hindbrain region. Scale bars indicate 50 μm.

body plan in class 3 and class 4 morphants (**Supplementary Fig. 4**). We next examined neural tube morphogenesis in control and httMO-injected embryos. Defects in httMO became apparent from somite stage 7–8, after the onset of neurulation, and persisted until 24 hours post-fertilization (hpf) (**Fig. 2a–d** and **Supplementary Fig. 5**). In particular, longitudinal sections of embryos at somite stage 10 (14 hpf) revealed that neural progenitor cells in the cephalic region were less clustered in httMO-treated embryos than in control embryos (**Fig. 2a**,**b**). Moreover, at 24 hpf, httMO-injected embryos displayed a compromised structure of the neural tube at the level of the diencephalons (**Fig. 2c**,**d** and **Supplementary Fig. 5**), with clusters of mispositioned cells and cellular aggregates in the ventricles (**Fig. 2d** and **Supplementary Fig. 5**). Furthermore, morphants displayed an altered brain ventricular space and a reduced cephalic region compared with control embryos (**Fig. 2e**,**f**). Expression domains of *wnt1*, which labels the prospective roof plate in the dorsal midbrain and hindbrain[28], and *atoh1*, which labels rhombomeric boundaries[29], were altered in httMO-injected embryos compared with control embryos (**Fig. 2g–j**), suggesting defects occurred in neural tube shaping and opening. Alteration of the *atoh1* expression domain suggests that the left and right side of the neural tube do not open uniformly in the hindbrain of httMO, consistent with our finding of abnormal neural tube shape (**Fig. 2e**,**f**). Finally, immunohistochemistry for ZO-1 in httMO-treated embroys at 24 hpf, a stage at which ZO-1 becomes enriched at the midline in anterior region of the developing neural tube, revealed either a disorganized (**Supplementary Fig. 5**) or reduced (data not shown) ZO-1 signal in neuroepithelial cells. These data suggest that the loss of htt leads to defects in neuroepithelial cell organization and apico-basal polarity during neurulation, which compromise the integrity of the neural tube.

htt regulates ADAM10/Ncadherin cell-anchoring mechanisms

We next tested whether the observed defects in neuroepithelial cell organization in the absence of htt could be linked to a defect in the motility of htt-null cells and performed time-lapse recording of $Hdh^{+/+}$ and Hdh^{ex4-5} cells during the process of rosettes formation. Cellular motility did not change significantly in htt-null cells ($Hdh^{+/+}$, 0.34 ± 0.03 μm min^{-1}; Hdh^{ex4-5}, 0.28 ± 0.03 μm min^{-1}; mean of two independent experiments, $P = 0.19$, two-tailed unpaired t test). We reasoned that htt may participate in cell-cell adhesion mechanisms that contribute to htt's function in neural rosette formation.

Ncadherin (cadherin2, Ncad) is a protein that is typically found in adherent junctions[30]. It is involved in the regulation of cell adhesion and migration in the CNS[30] and is essential for neurulation[31]. Its cleavage by ADAM10 regulates cell adhesion and this generates an N-terminal, 95-kDa fragment and a C-terminal, 40-kDa fragment (CTF1); CTF1 is processed further by the presenilin and γ-secretase complex into a soluble 35-kDa fragment (CTF2)[32,33]. We first tested whether Ncadherin functioned downstream of normal htt signaling by evaluating its expression in $Hdh^{+/+}$ and Hdh^{ex4-5} cells at day 8 of monolayer differentiation. We found no differences between genotypes in full-length Ncadherin levels (**Fig. 3a**). However, we observed a five-fold increase in the level of the CTF1 fragment present in Hdh^{ex4-5} compared with $Hdh^{+/+}$ cultures (**Fig. 3a**). This was confirmed in Hdh^{pr-ex1} neuroepithelial cells compared with $Hdh^{+/+}$ cells (**Fig. 3a**,**b**). CTF1 levels were significantly higher in Hdh^{ex4-5} cultures than in $Hdh^{+/+}$ cultures at earlier time points (days 5–7; $P < 0.05$ at day 5, $P < 0.01$ at days 6 and 7; **Supplementary Fig. 6**). As expected, Ncadherin was not expressed in self-renewing ES cells (day 0; **Supplementary Fig. 6**).

ADAM10 is the metalloprotease that is primarily responsible for Ncadherin cleavage[32]. Western blotting for ADAM10 in $Hdh^{+/+}$ cells (**Fig. 3c**) revealed the three expected immunoreactive bands of 100, 80 and 60 kDa, corresponding to the full-length ADAM10 precursor (full-length ADAM10), the partially processed (inactive) form (p-ADAM10) and the catalytically active protein (m-ADAM10), respectively. The amount of full-length ADAM10 was reduced at day 8 in Hdh^{ex4-5} cultures compared with $Hdh^{+/+}$ (**Fig. 3c**). Conversely, $Hdh^{ex4/5}$ cells had increased levels of m-ADAM10 and p-ADAM10 (**Fig. 3c**); in particular, m-ADAM10 expression was increased 3.0 ± 0.6–fold in Hdh^{ex4-5} compared with $Hdh^{+/+}$ cultures on day 8 (**Fig. 3c**). To determine whether the catalytic portion of ADAM10 was irreversibly compromised in htt-null cells, we treated Hdh^{ex4-5} cultures with the tissue inhibitor of MMP-1 (TIMP1), an ADAM10 inhibitor. We found that the formation of CTF1 was prevented in

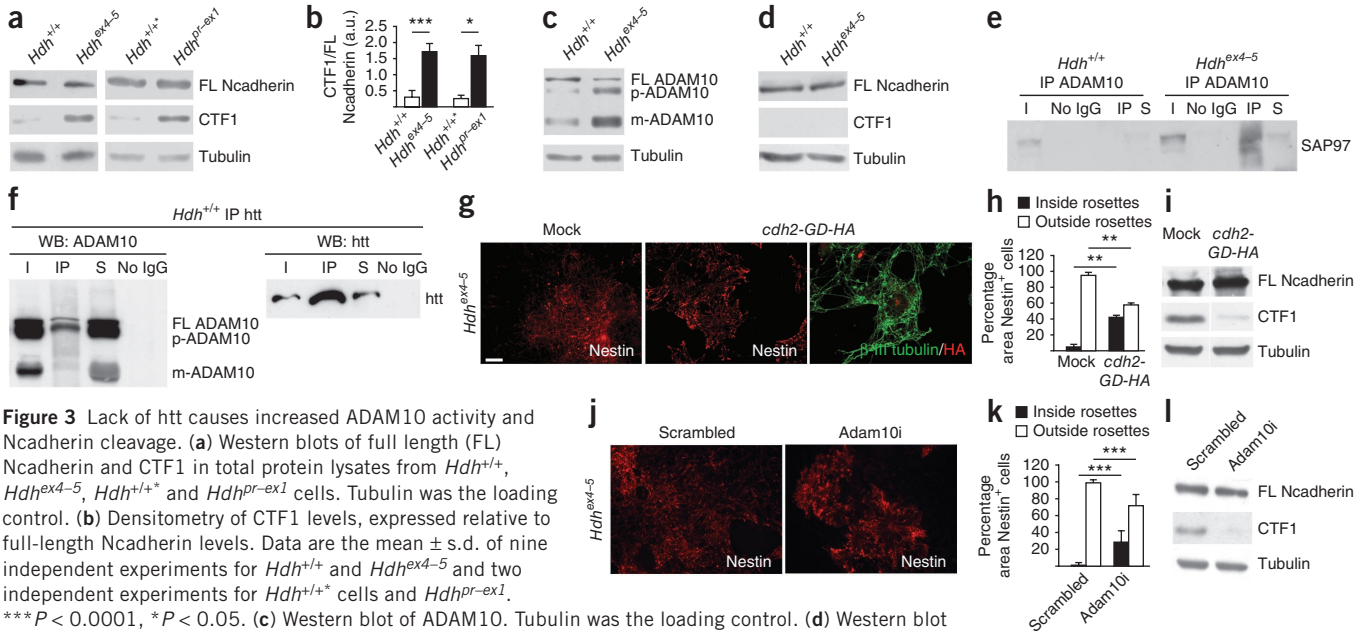

Figure 3 Lack of htt causes increased ADAM10 activity and Ncadherin cleavage. (**a**) Western blots of full length (FL) Ncadherin and CTF1 in total protein lysates from *Hdh*$^{+/+}$, *Hdh*$^{ex4–5}$, *Hdh*$^{+/+*}$ and *Hdh*$^{pr–ex1}$ cells. Tubulin was the loading control. (**b**) Densitometry of CTF1 levels, expressed relative to full-length Ncadherin levels. Data are the mean ± s.d. of nine independent experiments for *Hdh*$^{+/+}$ and *Hdh*$^{ex4–5}$ and two independent experiments for *Hdh*$^{+/+*}$ cells and *Hdh*$^{pr–ex1}$. $***P < 0.0001$, $*P < 0.05$. (**c**) Western blot of ADAM10. Tubulin was the loading control. (**d**) Western blot for full-length Ncadherin and CTF1 after treatment with 34 μM TIMP1, an ADAM10 inhibitor. (**e**) ADAM10-SAP97 complex in *Hdh*$^{+/+}$ and *Hdh*$^{ex4–5}$ cells. Antibody to ADAM10 was used for immunoprecipitation and the membrane was blotted with antibody to SAP97. I, input; IP, immunoprecipitation; S, immunoprecipitation supernatant. (**f**) Interaction between endogenous htt and ADAM10 determined by co-immunoprecipitation experiments. Antibody to htt (Mab2166) was used for the immunoprecipitation and the membrane was blotted with antibody to ADAM10. The same membrane exposed to antibody to htt as control for htt immunoprecipitation. (**g**) Immunostaining with Nestin, β-III tubulin and HA at day 8 of neural differentiation of *Hdh*$^{ex4–5}$ cells overexpressing full-length mutant (ADAM10 resistant) Ncadherin (*cdh2-GD-HA*). (**h**) Quantification of Nestin$^+$ cells inside and outside of neural rosettes in *Hdh*$^{ex4–5}$ cells overexpressing *cdh2-GD-HA* and parental cells (*Hdh*$^{ex4–5}$). Data are the mean ± s.e.m. of two independent experiments. $**P < 0.01$. (**i**) Western blots of full-length Ncadherin and CTF1 in *Hdh*$^{ex4–5}$ cells overexpressing *cdh2-GD-HA*. (**j**) *Hdh*$^{ex4–5}$ cells transfected with *Adam10* siRNA (Adam10i) or scrambled siRNA immunostained for Nestin at day 8 of neural differentiation. (**k**) Quantification of Nestin$^+$ cells inside and outside of neural rosettes after transfecting with scrambled siRNA or *Adam10* siRNA in *Hdh*$^{ex4–5}$ cells. Data are the mean ± s.e.m. of two independent experiments. (**l**) Western blots for full-length Ncadherin and CTF1 in *Hdh*$^{ex4–5}$ cells exposed to *Adam10* or scrambled siRNA. *P* values were evaluated with the unpaired two-tailed *t* test. Scale bar indicates 75 μm. See **Supplementary Figure 10** for full-length pictures of the blots.

htt-null cells (**Fig. 3d**). These data suggest that htt controls ADAM10-mediated cleavage of Ncadherin during rosettes formation.

Interaction with synapse-associated protein 97 (SAP97) promotes ADAM10 trafficking to the plasma membrane[34,35]. The association of ADAM10 and SAP97 positively modulates ADAM10 activity and Ncadherin cleavage[34,35]. On this basis, we investigated whether increased Ncadherin cleavage in the absence of htt was paralleled by increased formation of the ADAM10-SAP97 complex. Although the ADAM10-SAP97 complex was undetectable in *Hdh*$^{+/+}$ cells at day 8 of the neurulation protocol, the complex formed in *Hdh*$^{ex4–5}$ cells, as revealed by immunoprecipitation with an antibody to ADAM10 followed by western blotting with antibody to SAP97 (**Fig. 3e**). ADAM10 (mRNA) and SAP97 (mRNA and protein) levels were similar in the two genotypes (**Supplementary Fig. 7**). To test the possibility that htt may interact with ADAM10, we immunoprecipitated total protein lysates from *Hdh*$^{+/+}$ at day 8 with antibody to htt and immunoblotted with antibody to ADAM10 (**Fig. 3f**). ADAM10 co-immunoprecipitated with endogenous htt (**Fig. 3f**), indicating that htt interacts directly or indirectly with ADAM10 to control ADAM10-dependent cleavage of Ncadherin and neuroepithelial cell adhesion. Overexpression of an HA-tagged mutant Ncadherin transgene (*cadherin 2*, *cdh2*) resistant to ADAM10 cleavage (*cdh2-GD-HA*)[36] was able to partially rescue the rosetteless phenotype of *Hdh*$^{ex4–5}$ cells (% of Nestin$^+$ cells inside rosettes: *Hdh*$^{ex4–5}$ transfected with *cdh2-GD-HA*, 42.25 ± 2.37; *Hdh*$^{ex4–5}$ mock, 4.7 ± 3.35; **Fig. 3g**,**h**). This result was accompanied by a 9.7 ± 0.4–fold reduction in CTF1 fragment production in the partially rescued cells (**Fig. 3i**). We also found that transient knockdown of *Adam10* with siRNA in *Hdh*$^{ex4–5}$ cells (**Supplementary Fig. 2**) caused incorporation of 28.32 ± 13.37% of Nestin$^+$ cells inside the rosettes (**Fig. 3j**,**k**) and a concomitant 14.00 ± 0.13–fold decrease in the CTF1 levels (**Fig. 3l**). These data further confirm that idea htt's control over neural rosette formation depends on the regulation of Ncadherin cleavage by preventing the formation of the ADAM10-SAP97 complex, which leads to a decrease in the expression of the activated form of ADAM10 at the plasma membrane.

We next tested the link between htt and Ncadherin and ADAM10 *in vivo*. Western blot analyses indicated that level of cleaved Ncadherin product was 2.6 ± 0.2–fold higher in httMO-treated zebrafish embryos than in control (**Fig. 4**). This was consistent with an approximately two fold lower level of unprocessed Ncadherin in htt-null morphants compared with control embryos.

To further demonstrate that htt loss-of-function alters the adhesiveness of neuroectodermal cells during neurulation by influencing Ncadherin functionality, we analyzed those neural markers affected in the zebrafish *parachute* mutants, which carry potential null mutations in a zebrafish Ncadherin homolog. In *parachute* mutants, the loss of neural tube organization is restricted to alar regions whereas cells in the basal positions remain correctly organized[37]. In our htt knockdown zebrafish embryos at somite stage 2–3, as is also seen in *parachute* mutants[37], the expression patterns of the floor plate marker *shh*, the alar-basal marker *pax2.1* and the roofplate marker *wnt1*, were indistinguishable from control embryos (**Fig. 5a–f**). In htt loss-of-function embryos, as well as in *parachute* mutants, the loss of neural tube organization became evident from somite stage

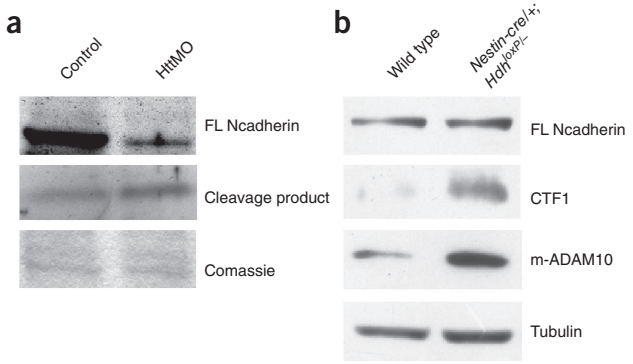

Figure 4 Ncadherin cleavage and ADAM10 activity in the zebrafish and mouse brain. (**a**) Western blots for Ncadherin (full length and cleaved form) in total protein lysates from controls and httMO-treated zebrafish embryos at 24 hpf. Comassie blue stain shows loading control. (**b**) Western blots of Ncadherin (full length and CTF1) and ADAM10 in *Nestin-cre/+; Hdh*$^{loxP/–}$ mouse brains and brains of control littermates ($n = 2$ for each genotype). See **Supplementary Figure 10** for full-length pictures of the blots.

7–8 to the complete formation of the neural tube at 24 hpf (**Fig. 5g–l** and **Fig. 2g–j**) and was restricted to alar regions, as shown by alar *pax2.1* (**Fig. 5i,j**) and *wnt1* mis-expression (**Fig. 5k,l**). Cells in the basal positions remained correctly organized (see *shh* and basal *pax2.1* expression patterns; **Fig. 5g–j**). We conclude that htt knockdown in zebrafish embryos phenocopies *parachute* mutants and that neuroepithelial cell-cell adhesion and morphogenesis of the neural tube in zebrafish depends on htt's control over Ncadherin activity.

GI254023X is a mammalian ADAM10 blocker that has been successfully used in mice[38] and in organisms that are evolutionarily close to zebrafish[39]. Given that the amino acid sequence of the ADAM10 catalytic site is highly conserved between zebrafish and mice (89% amino acid identity), we used GI254023X to block ADAM10 in httMO zebrafish. Administration of 40 µM GI254023X for 24 h led to a substantial morphological rescue of the httMO-treated embryos, as shown by the shift toward the less affected class 1 and 2 morphants (**Fig. 6a–e**). Moreover, GI254023X-treated embryos displayed a substantial reduction in the neural tube shape defects that were observed in morphants with only a few cells being found in the ventricular spaces (**Fig. 6f–k**).

These data support the notion that htt regulates neurulation *in vivo* by controlling ADAM10 activity. Consistent with this, we found an approximately 2.1 ± 0.5-fold increase in the expression m-ADAM10 in the brains of htt conditional knockout mice (*Nestin-cre/+; Hdh*$^{loxP/–}$ mice) at 1.75 months of age, as compared with controls (**Fig. 4**). This resulted in a 7.7 ± 1.6–fold increase in the level of CTF1 (**Fig. 4**). We conclude that htt can regulate ADAM10-mediated Ncadherin cleavage in the mature mouse brain.

htt has acquired cell-adhesion function during evolution

We next investigated whether a specific domain in htt confers control of cell-cell adhesion during mammalian neurulation. We focused on the ~500 amino acid N-terminal portion of htt[11], as it has evolved more recently based on its divergence from *Ciona intestinalis* and *Drosophila melanogaster* htt, which lack the polyQ motif[2]. In contrast, the 650 amino acid C terminus of htt is highly conserved among all animals[2]. Notably, we found that constitutive expression of the 548 amino acid N terminus of mouse htt (*Mus musculus*) in *Hdh*$^{ex4–5}$ cells nearly completely rescued the rosetteless phenotype (**Fig. 7a,b**). No rescue was observed when the 650 amino acid C terminus of htt was constitutively expressed (**Fig. 7a,b**). These data indicate that the N terminus of htt confers neural cell-adhesion properties. Moreover, subclones of *Hdh*$^{ex4–5}$ cells that expressed different amounts of the htt N terminus derived from *M. musculus* or *Homo sapiens* (**Supplementary Fig. 8**) were all able to form neural rosettes (**Supplementary Fig. 8**), indicating that the transgene dose was saturating.

We next investigated whether htt pro-rosette activity was present in ancestral organisms from the lower parts of the evolutionary tree. We performed complementation assays in *Hdh*$^{ex4–5}$ cells by expressing N-terminal htt fragments derived from ancient and more recently evolved species in the deuterostome and protostome branches (**Supplementary Fig. 9**). In particular, we tested htt from *D. discoideum* (N569 portion), a motile soil amoeba with no nervous system that emerged at the point of transition from unicellular to multicellular organisms, from the echinoderm, *S. purpuratus* (N519 portion), which has a primitive nervous system organized into a radial nerve, from the tunicate *C. intestinalis* (N409 portion), a chordate-invertebrate that has a body plan and embryonic development very similar to those of vertebrates, but is highly divergent at the adult stage from vertebrates in the structure of the nervous system, from the cephalochordate, lancelet *Branchiostoma floridae* (N478 portion), whose nervous system represents a first attempt of cephalization with an antero-posterior polarity, and from *D. rerio* (N517 portion), a vertebrate species. For controls, we included htt from *M. musculus* (N548 portion), *H. sapiens* (N652 portion) and a protostome, *D. melanogaster* (N548 portion), which follows a different type of developmental program for the structuring of its nervous system.

The cDNAs that encoded the htt N termini from *D. discoideum*, *S. purpuratus*, *C. intestinalis*, *B. floridae*, *D. rerio* and *D. melanogaster* were tagged with hemagglutinin (HA tag) and transfected into *Hdh*$^{ex4–5}$ ES cells to generate stable *Hdh*$^{ex4–5}$ ES cell lines. Immunocytochemical and western blotting analyses with antibodies to htt and HA confirmed the expression of the exogenous protein(s) in the different cell lines (**Supplementary Fig. 9**). We then

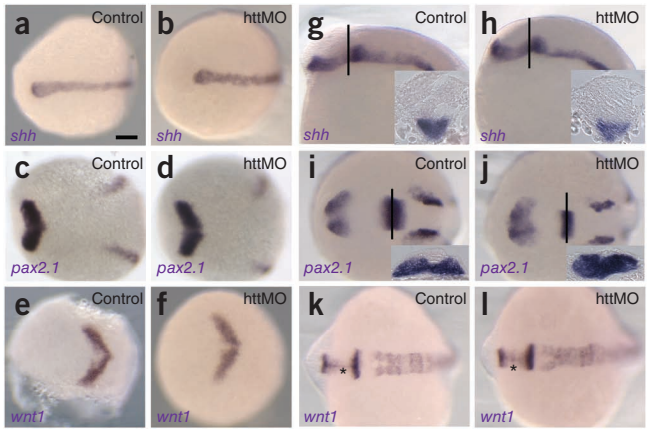

Figure 5 Effects of htt loss-of-function during neurulation. (**a–f**) Whole-mount *in situ* hybridization for *shh*, *pax2.1* and *wnt1* at somite stage 2–3. *shh*, *pax2.1* and *wnt1* were expressed in indistinguishable patterns in control and morphant embryos. (**g–l**) Whole-mount *in situ* hybridization for the markers *shh* and *pax2.1* and *wnt1* at somite stage 7–8. The floor plate marker *shh* (**g,h**, insets) and basal expression of *pax2.1* (**i,j**, insets) were unaltered in morphants. Alar expression of *pax2.1* (**i,j**, insets) and expression of *wnt1* (asterisks) in the roofplate (**k,l**) were altered in httMO-injected embryos with respect to controls. Black lines indicate the locations of cross-sections in the insets. Scale bar represents 100 µm.

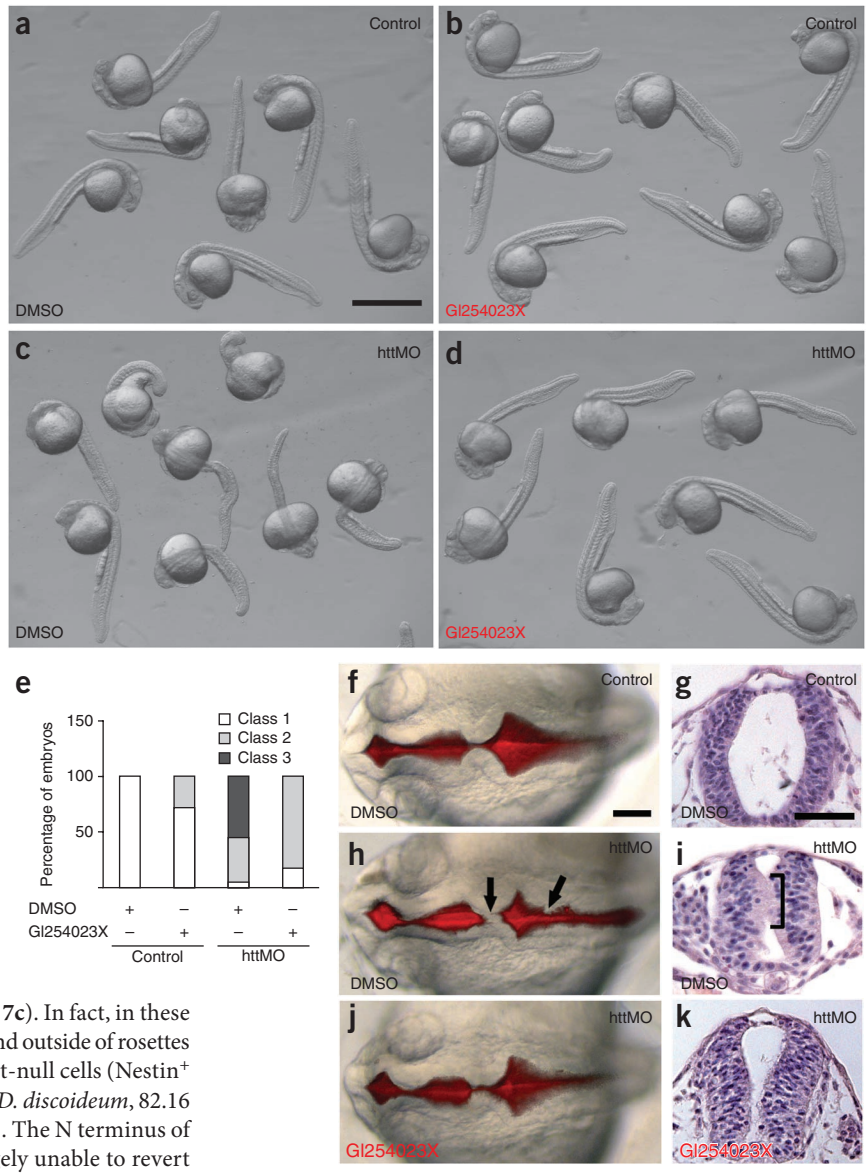

Figure 6 The block of ADAM10 activity partially rescued httMO phenotypes at 24 hpf. (**a**,**b**) Both DMSO- and GI254023X-treated control embryos had normal morphology. (**c**) DMSO-treated httMO presented a strongly affected overall morphology at 24 hpf as a result of htt knockdown. (**d**) Structural defects of morphants were partially rescued by the application of 40 μM GI254023X into the fish water. (**e**) Histogram shows the trend of a representative GI254023X treatment in which the block of ADAM10 activity determined the shift of the most affected phenotypic class 3 morphants toward the less affected phenotypic class 1 and 2 morphants; one of three independent experiments is shown that gave the same results. (**f**,**h**,**j**) Control, httMO-treated and httMO-GI254023X–treated embryos injected with rhodamine and dextran at 24 hpf. (**g**,**i**,**k**) Cross-sections of the neural tube in control, httMO-treated and httMO-GI254023X–treated embryos (class 1 and 2) at 24 hpf stained with haematoxylin and eosin. Defects in ventricular space and shape of httMO-treated embryos were partially recovered in 30% of the GI254023X-treated morphants. In particular, a significant reduction of mis-positioned cells was observed in the brain ventricles (black arrows in **h** and bracket in **i**). Scale bars represent 500 μm (**a**–**d**) and 100 μm (**f**–**k**).

subjected the cell lines to a monolayer differentiation protocol[26] and, on day 8, stained the cells for Ncadherin and Nestin. Notably, N-terminal htt proteins from distant species, including *D. discoideum* or *D. melanogaster*, were unable to complement the rosetteless phenotype when expressed in Hdh^{ex4-5} cells (**Fig. 7c**). In fact, in these cultures, the vast majority of Nestin$^+$ cells were found outside of rosettes (**Fig. 7d**), similar to observations in cultures of htt-null cells (Nestin$^+$ cells outside the rosettes: Hdh^{ex4-5}, 95.03 ± 3.56%; *D. discoideum*, 82.16 ± 9.21%; *D. melanogaster*, 84.58 ± 2.00%; **Fig. 7d**). The N terminus of *S. purpuratus* and *C. intestinalis* htt was also largely unable to revert the rosetteless phenotype (Nestin$^+$ cells outside the rosettes: *S. purpuratus*, 79.37 ± 4.12%; *C. intestinalis*, 76.98 ± 6.33%; **Fig. 7d**), although a few low-quality rosettes (that is, radially arranged neuroepithelial cells without a defined lumen and polarity) could be found. In contrast, transfection of htt from the more recently evolved species, *B. floridae*, *D. rerio*, *M. musculus* and *H. Sapiens*, consistently resulted in a statistically significant and progressive reduction in the area occupied by Nestin$^+$ cells outside of the rosettes compared with Hdh^{ex4-5} cells (*B. floridae*, 61.64 ± 4.96%; *D. rerio*, 51.62 ± 1.5%; *M. musculus*, 28.25 ± 1.16%; *H. sapiens*, 22.80 ± 8.98%; $P < 0.0001$, with respect to Hdh^{ex4-5} cells, according to one-way ANOVA with post-test Bonferroni; **Fig. 7d**). We also determined the size of rosettes by measuring the longer diameter at day 8. Rosettes were classified as normal size (that is, diameter > 150 μm) and small (80 < diameter < 150 μm). We observed that, also correlating with deuterostome evolution, the size of rosettes gradually increased in the following order: *D. melanogaster* = *D. discoideum* < *S. purpuratus* = *C. Intestinalis* < *B. floridae* = *D. Rerio* < *M. musculus* = *H. sapiens* (**Fig. 7e**). Accordingly, the propensity of Ncadherin cleavage, judged by CTF1 levels, decreased proportionally in Hdh^{ex4-5} cells that expressed htt from progressively more recently evolved species (**Fig. 7f**). In contrast, no substantial differences in Ncadherin cleavage were observed among *D. melanogaster*, *D. discoideum*, *S. purpuratus*, *C. intestinalis* and null controls when normalized on tubulin levels (Hdh^{ex4-5} cells; **Fig. 7f**). Densitometric analyses on three independent western blots indicated that htt from *B. floridae*, *D. rerio*, *M. musculus* and *H. sapiens* showed 3.3 ± 0.3, 8.0 ± 2.0, 8.6 ± 2.6 and 21.2 ± 7.0–fold decreases, respectively, in CTF1 production compared with Hdh^{ex4-5} cells (**Fig. 7f**,**g**). Notably, the N terminus of both *D. melanogaster* and *D. discoideum* htt did not complement the rosetteless phenotype. On the basis of these data, we conclude that htt's control of cell adhesion is an evolutionarily recent acquisition of the protein that is specific to deuterostome organisms.

Previous studies have found that mammalian htt has an anti-apoptotic effect in neural and non-neural cells *in vitro*[11–13] and in brain[7,8]. This activity is embedded in the htt 548 amino acid N terminus[11]. We investigated whether htt's anti-apoptotic activity is an ancestral or recent acquisition. To test this, we serum-deprived Hdh^{ex4-5} lines that stably expressed the N-terminal portions of htt homologs. In previous studies, this experimental condition led to an approximately 40% increase in caspase-3 activation in Hdh^{ex4-5} cells

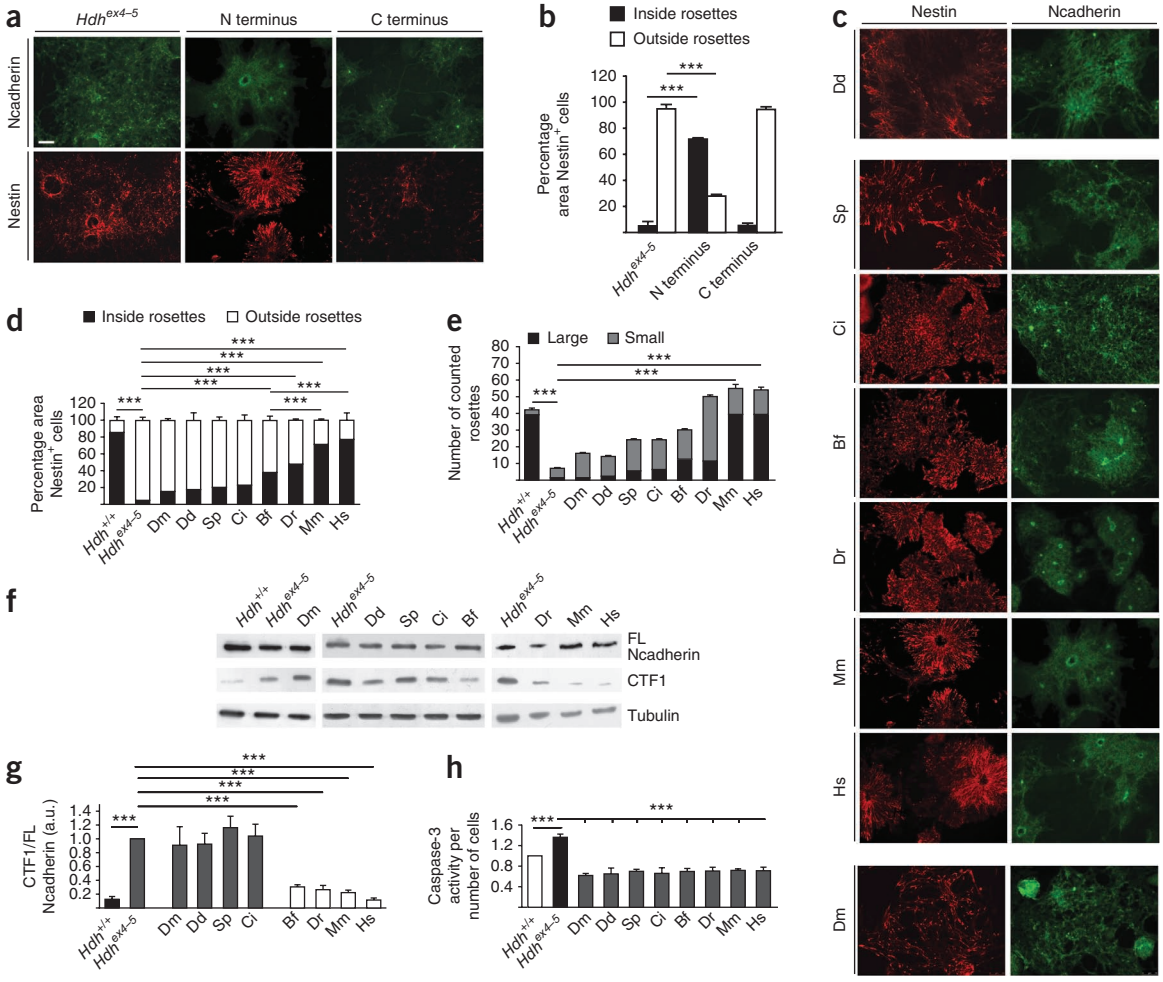

Figure 7 htt N terminus neural cell-adhesion function during evolution. (**a**) *Hdh*$^{ex4–5}$ cells stably expressing the N terminus or C terminus of htt from *M. musculus* were immunostained for Ncadherin and Nestin on day 8 of monolayer differentiation. (**b**) Quantification of Nestin$^+$ cells in *Hdh*$^{ex4–5}$ cells expressing N-terminal or C-terminal fragments and parental cells. Data are the mean ± s.d. from three independent experiments. ***$P < 0.0001$. (**c**) Immunostaining for Ncadherin and Nestin in *Hdh*$^{ex4–5}$ cells stably expressing htt N terminus from *D. discoideum* (Dd), *S. purpuratus* (Sp), *C. intestinalis* (Ci), *B. floridae* (Bf), *D. rerio* (Dr), *M. musculus* (Mm), *H. sapiens* (Hs) or *D. melanogaster* (Dm). (**d**) Quantification of Nestin$^+$ cells inside and outside of rosettes. (**e**) Mean rosette sizes. Data are the mean ± s.d. of three independent experiments. (**f**) Western blots for full length Ncadherin and CTF1 in *Hdh*$^{ex4–5}$ cells overexpressing htt N terminus from *D. discoideum*, *S. purpuratus*, *C. intestinalis*, *B. floridae*, *D. rerio*, *M. musculus*, *H. sapiens* and *D. melanogaster*. (**g**) Densitometry of CTF1 relative to full-length Ncadherin. Data are the mean ± s.d. of three independent experiments. (**h**) Caspase-3 activity in *Hdh*$^{ex4–5}$ cells expressing N-terminal *D. discoideum*, *S. purpuratus*, *C. intestinalis*, *B. floridae*, *D. rerio*, *M. musculus*, *H. sapiens* and *D. melanogaster* htt. Data are the mean ± s.d. of three independent experiments. All *P* values were evaluated with one-way ANOVA with post-test Bonferroni. Scale bar indicates 75 μM. See **Supplementary Figure 10** for full-length pictures of the blots.

compared with controls[40]. We also found that caspase-3 activity was significantly increased in *Hdh*$^{ex4–5}$ cells compared with *Hdh*$^{+/+}$ cells ($P < 0.0001$, one-way ANOVA with post-test Bonferroni; **Fig. 7h**). In contrast, when *Hdh*$^{ex4–5}$ cells overexpressed any of the N-terminal htt from ancient and more evolved species, they were significantly protected from apoptosis induced by serum deprivation ($P < 0.0001$, one-way ANOVA with post-test Bonferroni). The extent of rescue was similar among cells that expressed different htt orthologs; this suggests that htt's anti-apoptotic activity is an ancestral function that appeared in *D. discoideum* and was maintained in *H. sapiens* and *D. melanogaster*. In conclusion, our results indicate that htt possesses two functions that are embedded in its N terminus: the prevention of apoptosis, which is present in ancestral genes, and the control of cell-cell contacts between neuroepithelial cells, which is an evolutionarily more recent acquisition.

DISCUSSION

Taking advantage of an ES cell–based neural differentiation protocol[26], we found that htt is involved in homotypic interactions between neuroepithelial cells by regulating a critical cell-cell adhesion pathway involving ADAM10 and Ncadherin activities. The ablation of Ncadherin in mouse and zebrafish embryos causes a defect in neural tube formation[31,37]. We found that blocking htt transcript in zebrafish embryos resulted in impaired Ncadherin-mediated cell-cell interactions and impaired expression and distribution of the apical marker ZO-1, which in turn result in cell dispersion and cellular aggregates in the brain ventricles during development. Notably, we found that, in htt loss-of-function embryos and Ncadherin mutants, the loss of neural tube organization was restricted to alar regions, whereas cells in the basal positions remain correctly organized[37]. These data support the notion that neurulation defects in the htt knockdown zebrafish

embryos depend on impairment in Ncadherin-mediated cell adhesion. We observed a similar cell-cell interaction defect, which we termed rosetteless, in htt-null ES cells that were undergoing neurulation. This defect was rescued by the expression of an Ncadherin mutant that lacked the ADAM10 cleavage site or with transfection of ADAM10 siRNA. Similarly, inhibition of ADAM10 activity by pharmacological treatment *in vivo* improved the overall morphology and brain ventricle shape of htt loss-of-function zebrafish embryos. Furthermore, our results suggest a mechanistic model in which wild-type htt controls cell-adhesion functions by recruiting ADAM10 in the cell cytoplasm, thereby regulating the formation of the ADAM10-SAP97 complex that drives Ncadherin cleavage. ADAM10 is responsible for the shedding of several cell surface proteins in addition to Ncadherin. Ephrins, amyloid precursor protein and Notch are some of the growing list of ADAM10 substrates that are involved in brain development[41,42]. It is possible that htt may regulate the activity of other ADAM10 substrates.

We also found that htt's control of neural cell adhesion is an evolutionarily recent acquisition in deuterostomes and is associated with the N terminus of the protein. This function was subtle in lower deuterostomes and then appeared in the cephalochordate *B. floridae*, the first organism to exhibit cephalization, and increased in fishes and mammals. It is highly likely that, beyond cell adhesion, additional htt activities and molecular pathways could emerge during evolution to further reinforce htt's role during neurulation in mammals. Furthermore, *D. melanogaster* htt did not exhibit this cell-adhesion function, which suggests that htt's neural function in *D. melanogaster* may be fundamentally different or limited. Accordingly, the *D. melanogaster* htt sequence is quite divergent from mammalian htt[2,43] and, in contrast with observations in mice, the htt knockout flies showed no obvious developmental defects[44]. We also found that the N-terminal domain of htt confers cell-adhesion activities that are essential for neurulation. Notably, all eight of the heterologous N-terminal htt constructs that we tested were equally capable of reverting apoptosis in self-renewing htt-null ES cells exposed to serum deprivation. We propose that the anti-apoptotic activity of htt may represent one of htt's ancestral function(s). htt's ability to control mitotic spindle orientation was also acquired early in evolution and is conserved in *D. melanogaster*[22]. However, we found that, later in deuterostome evolution, htt acquired a more specific neural cell-adhesion regulation activity, with implications for brain development in vertebrates.

We also found increased ADAM10 activity and Ncadherin cleavage in htt-deficient adult brain, which suggests that htt may control cell-cell adhesion in the mature brain, perhaps to promote neuronal plasticity or synapse remodeling. An increase in the activity of other matrix metalloproteinases has been seen in the brains of individuals afflicted with Huntington's disease[45]. ADAM10 and Ncadherin were previously implicated in spine maturation[35]; increased ADAM10 activity was associated with protection from neurodegeneration in mouse models of Alzheimer Disease[46,47]; and total Ncadherin levels were reduced in cellular and mouse model of Huntington's disease[48]. Our findings reveal a previously unknown function for htt during neurulation and suggest that the progressive increase in the length of its CAG repeat sequence in deuterostomes may be implicated in the evolutionary path that has led to the acquisition of morphological complex nervous systems. Our findings indicate that evolutionary principles can be experimentally tested and suggest ADAM10 as a new target in the treatment of Huntington's disease.

METHODS

Methods and any associated references are available in the online version of the paper at http://www.nature.com/natureneuroscience/.

Note: Supplementary information is available on the Nature Neuroscience website.

ACKNOWLEDGMENTS

We thank M. MacDonald (Massachusetts General Hospital) for the $Hdh^{+/+}$ and Hdh^{ex4-5} cells, P. Saftig for the ADAM10 antibody (University of Kiel), E. Ruthazer for the zebrafish Ncadherin antibody (McGill University), F. Gardoni and E. Marcello for helpful technical advice on the use of ADAM10 and SAP97 antibodies, A. Badaloni for help with subcloning, and G. Simonutti for assistance with initial imaging analysis. This work has progressed at a very slow pace because it was mostly unfunded. In the beginning, this work was partially supported by the Huntington's Disease Society of America Coalition for the Cure (2007–2009) and by Italian Telethon Foundation (GGP06250, 2007–2009). Some additional support was provided by the Ministero dell'Istruzione, dell'Università e della Ricerca Scientifica, Programmi di Ricerca Scientifica di Rilevante Interesse Nazionale (2006052993, 2006). Since 2009, progress of this work has relied entirely on occasional donations. We wish to thank one donor that in 2009 collected a considerable amount of small donations for us to continue this work and another donor that has been following our progress for 10 years. C.R. was supported by the Fundação para a Ciência e Tecnologia (grant number SFRH/BD/9627/2002) through the GABBA Programme (University of Porto). E.C., J.G. and S.Z. were members of the Huntington's Disease Society of America Coalition for the Cure and J.G. received support from NS16367.

AUTHOR CONTRIBUTIONS

E.C., V.L.S. and C.Z. developed the study, conceived the experimental plans and analyzed the data. V.L.S. and C.Z. performed most of the biological, biochemical and molecular experiments. B.V. performed some of the biological and biochemical experiments. M.T. and C.R. participated in the initial elaboration of the project and conducted some experiments (some of the initial constructs preparation and monolayer assays, respectively). V.L.S. prepared additional constructs. M.A.M., J.A.W. and J.G. provided the *Dictyostelium* and *Drosophila* cDNA. G.G., C.Z. and A.P. performed experiments in zebrafish under the supervision of F.C. (immunocytochemistry and *in situ* were performed by G.G. and A.P., biochemical assays by C.Z.). M.V. and L.C. provided suggestions for some biological experiments. S.Z. provided the conditional knockout mice and some constructs. B.D. and B.S. provided GI254023X. V.L.S., C.Z. and E.C. interpreted the data and wrote the manuscript. All of the authors read and edited the manuscript. E.C. supervised the entire work, directed the strategies, provided financial support and gave final approval of the version to be published.

COMPETING FINANCIAL INTERESTS

The authors declare no competing financial interests.

Published online at http://www.nature.com/natureneuroscience/.
Reprints and permissions information is available online at http://www.nature.com/reprints/index.html.

1. MacDonald, M.E. *et al.* A novel gene containing a trinucleotide repeat that is expanded and unstable on Huntington's disease chromosomes. *Cell* **72**, 971–983 (1993).
2. Tartari, M. *et al.* Phylogenetic comparison of huntingtin homologues reveals the appearance of a primitive polyQ in sea urchin. *Mol. Biol. Evol.* **25**, 330–338 (2008).
3. Palidwor, G.A. *et al.* Detection of alpha-rod protein repeats using a neural network and application to huntingtin. *PLoS Comput. Biol.* **5**, e1000304 (2009).
4. Myre, M.A. *et al.* Deficiency of huntingtin has pleiotropic effects in the social amoeba Dictyostelium discoideum. *PLoS Genet.* **7**, e1002052 (2011).
5. Bhide, P.G. *et al.* Expression of normal and mutant huntingtin in the developing brain. *J. Neurosci.* **16**, 5523–5535 (1996).
6. Zuccato, C., Valenza, M. & Cattaneo, E. Molecular mechanisms and potential therapeutical targets in Huntington's disease. *Physiol. Rev.* **90**, 905–981 (2010).
7. O'Kusky, J.R., Nasir, J., Cicchetti, F., Parent, A. & Hayden, M.R. Neuronal degeneration in the basal ganglia and loss of pallido-subthalamic synapses in mice with targeted disruption of the Huntington's disease gene. *Brain Res.* **818**, 468–479 (1999).
8. Dragatsis, I., Levine, M.S. & Zeitlin, S. Inactivation of Hdh in the brain and testis results in progressive neurodegeneration and sterility in mice. *Nat. Genet.* **26**, 300–306 (2000).
9. Zhang, Y. *et al.* Depletion of wild-type huntingtin in mouse models of neurologic diseases. *J. Neurochem.* **87**, 101–106 (2003).
10. Leavitt, B.R. *et al.* Wild-type huntingtin protects neurons from excitotoxicity. *J. Neurochem.* **96**, 1121–1129 (2006).
11. Rigamonti, D. *et al.* Wild-type huntingtin protects from apoptosis upstream of caspase-3. *J. Neurosci.* **20**, 3705–3713 (2000).
12. Rigamonti, D. *et al.* Huntingtin's neuroprotective activity occurs via inhibition of procaspase-9 processing. *J. Biol. Chem.* **276**, 14545–14548 (2001).

13. Ho, L.W., Brown, R., Maxwell, M., Wyttenbach, A. & Rubinsztein, D.C. Wild-type Huntingtin reduces the cellular toxicity of mutant Huntingtin in mammalian cell models of Huntington's disease. *J. Med. Genet.* **38**, 450–452 (2001).
14. Duyao, M.P. *et al.* Inactivation of the mouse Huntington's disease gene homolog *Hdh*. *Science* **269**, 407–410 (1995).
15. Nasir, J. *et al.* Targeted disruption of the Huntington's disease gene results in embryonic lethality and behavioral and morphological changes in heterozygotes. *Cell* **81**, 811–823 (1995).
16. Zeitlin, S., Liu, J.P., Chapman, D.L., Papaioannou, V.E. & Efstratiadis, A. Increased apoptosis and early embryonic lethality in mice nullizygous for the Huntington's disease gene homologue. *Nat. Genet.* **11**, 155–163 (1995).
17. Dragatsis, I., Efstratiadis, A. & Zeitlin, S. Mouse mutant embryos lacking huntingtin are rescued from lethality by wild-type extraembryonic tissues. *Development* **125**, 1529–1539 (1998).
18. White, J.K. *et al.* Huntingtin is required for neurogenesis and is not impaired by the Huntington's disease CAG expansion. *Nat. Genet.* **17**, 404–410 (1997).
19. Auerbach, W. *et al.* The HD mutation causes progressive lethal neurological disease in mice expressing reduced levels of huntingtin. *Hum. Mol. Genet.* **10**, 2515–2523 (2001).
20. Henshall, T.L. *et al.* Selective neuronal requirement for huntingtin in the developing zebrafish. *Hum. Mol. Genet.* **18**, 4830–4842 (2009).
21. Reiner, A. *et al.* Neurons lacking huntingtin differentially colonize brain and survive in chimeric mice. *J. Neurosci.* **21**, 7608–7619 (2001).
22. Godin, J.D. *et al.* Huntingtin is required for mitotic spindle orientation and mammalian neurogenesis. *Neuron* **67**, 392–406 (2010).
23. Abranches, E. *et al.* Neural differentiation of embryonic stem cells *in vitro*: a road map to neurogenesis in the embryo. *PLoS ONE* **4**, e6286 (2009).
24. Elkabetz, Y. *et al.* Human ES cell–derived neural rosettes reveal a functionally distinct early neural stem cell stage. *Genes Dev.* **22**, 152–165 (2008).
25. Hoettecke, N., Ludwig, A., Foro, S. & Schmidt, B. Improved synthesis of ADAM10 inhibitor GI254023X. *Neurodegener. Dis.* **7**, 232–238 (2010).
26. Ying, Q.L., Stavridis, M., Griffiths, D., Li, M. & Smith, A. Conversion of embryonic stem cells into neuroectodermal precursors in adherent monoculture. *Nat. Biotechnol.* **21**, 183–186 (2003).
27. Diekmann, H. *et al.* Decreased BDNF levels are a major contributor to the embryonic phenotype of huntingtin knockdown zebrafish. *J. Neurosci.* **29**, 1343–1349 (2009).
28. Kelly, G.M. & Moon, R.T. Involvement of wnt1 and pax2 in the formation of the midbrain–hindbrain boundary in the zebrafish gastrula. *Dev. Genet.* **17**, 129–140 (1995).
29. Adolf, B., Bellipanni, G., Huber, V. & Bally-Cuif, L. atoh1.2 and beta3.1 are two new bHLH-encoding genes expressed in selective precursor cells of the zebrafish anterior hindbrain. *Gene Expr. Patterns* **5**, 35–41 (2004).
30. Halbleib, J.M. & Nelson, W.J. Cadherins in development: cell adhesion, sorting and tissue morphogenesis. *Genes Dev.* **20**, 3199–3214 (2006).
31. Radice, G.L. *et al.* Developmental defects in mouse embryos lacking N-cadherin. *Dev. Biol.* **181**, 64–78 (1997).
32. Reiss, K. *et al.* ADAM10 cleavage of N–cadherin and regulation of cell-cell adhesion and beta-catenin nuclear signaling. *EMBO J.* **24**, 742–752 (2005).
33. Marambaud, P. *et al.* A presenilin-1/gamma-secretase cleavage releases the E-cadherin intracellular domain and regulates disassembly of adherens junctions. *EMBO J.* **21**, 1948–1956 (2002).
34. Marcello, E. *et al.* Synapse-associated protein 97 mediates alpha-secretase ADAM10 trafficking and promotes its activity. *J. Neurosci.* **27**, 1682–1691 (2007).
35. Malinverno, M. *et al.* Synaptic localization and activity of ADAM10 regulate excitatory synapses through N-cadherin cleavage. *J. Neurosci.* **30**, 16343–16355 (2010).
36. Uemura, K. *et al.* Characterization of sequential N-cadherin cleavage by ADAM10 and PS1. *Neurosci. Lett.* **402**, 278–283 (2006).
37. Lele, Z. *et al.* parachute/n-cadherin is required for morphogenesis and maintained integrity of the zebrafish neural tube. *Development* **129**, 3281–3294 (2002).
38. Inoshima, I. *et al.* A Staphylococcus aureus pore-forming toxin subverts the activity of ADAM10 to cause lethal infection in mice. *Nat. Med.* **17**, 1310–1314 (2011).
39. Chen, Y.Y., Hehr, C.L., Atkinson-Leadbeater, K., Hocking, J.C. & McFarlane, S. Targeting of retinal axons requires the metalloproteinase ADAM10. *J. Neurosci.* **27**, 8448–8456 (2007).
40. Zhang, Y. *et al.* Huntingtin inhibits caspase-3 activation. *EMBO J.* **25**, 5896–5906 (2006).
41. Yang, P., Baker, K.A. & Hagg, T. The ADAMs family: coordinators of nervous system development, plasticity and repair. *Prog. Neurobiol.* **79**, 73–94 (2006).
42. Muraguchi, T. *et al.* RECK modulates Notch signaling during cortical neurogenesis by regulating ADAM10 activity. *Nat. Neurosci.* **10**, 838–845 (2007).
43. Li, Z., Karlovich, C.A., Fish, M.P., Scott, M.P. & Myers, R.M. A putative *Drosophila* homolog of the Huntington's disease gene. *Hum. Mol. Genet.* **8**, 1807–1815 (1999).
44. Zhang, S., Feany, M.B., Saraswati, S., Littleton, J.T. & Perrimon, N. Inactivation of *Drosophila* Huntingtin affects long-term adult functioning and the pathogenesis of a Huntington's disease model. *Dis. Model Mech.* **2**, 247–266 (2009).
45. Miller, J.P. *et al.* Matrix metalloproteinases are modifiers of huntingtin proteolysis and toxicity in Huntington's disease. *Neuron* **67**, 199–212 (2010).
46. Postina, R. *et al.* A disintegrin-metalloproteinase prevents amyloid plaque formation and hippocampal defects in an Alzheimer disease mouse model. *J. Clin. Invest.* **113**, 1456–1464 (2004).
47. Prinzen, C. *et al.* Differential gene expression in ADAM10 and mutant ADAM10 transgenic mice. *BMC Genomics* **10**, 66 (2009).
48. Reis, S.A. *et al.* Striatal neurons expressing full-length mutant huntingtin exhibit decreased N-cadherin and altered neuritogenesis. *Hum. Mol. Genet.* **20**, 2344–2355 (2011).

ONLINE METHODS

Cell lines. We used mouse ES cell lines expressing either the wild-type huntingtin gene (*Hdh*$^{+/+}$ and *Hdh*$^{+/+*}$, two different batches of *Hdh*$^{+/+}$ ES cells) or carrying a homozygous knockout of the *Hdh* gene (*Hdh*$^{ex4-5}$, in which both alleles of the *Hdh* gene were inactivated by deletion of exons 4 and 5 (ref. 14); *Hdh*$^{pr\text{-}ex1}$, derived by deleting the promoter and exon 1 of the *Hdh* gene[16]).

Mouse ES cell culture. ES cells were maintained in Glasgow minimal essential medium supplemented with 10% heat-inactivated fetal bovine serum (vol/vol, EuroClone), 1 mM β-mercaptoethanol, 100 μM non-essential amino acids, 1 mM sodium pyruvate (Gibco), 2 mM L-glutamine, 100 U ml^{-1} penicillin, 100 μg ml^{-1} streptomycin (EuroClone) and 1,000 U ml^{-1} murine leukemia inhibitor factor (LIF, ESGRO) (Chemicon) in gelatinized tissue culture flasks. Cells were passaged every 2 d after dissociation with 0.05% trypsin-EDTA (vol/vol).

Mouse ES cell monolayer differentiation. ES cells were dissociated and plated onto 0.1% gelatin-coated tissue culture dishes at a density of 1–1.5 × 10^4 cells per cm^2 in N2B27 medium. Medium was renewed every 2 d. N2B27 medium was a 1:1 mixture of DMEM/F12 supplemented with N2 and Neurobasal medium supplemented with B27 (Gibco). After day 9, N2B27 cell culture medium was a 1:4 mixture of the same supplemented media.

Zebrafish lines and maintenance. Current Italian national rules: no approval needs to be given for research on zebrafish embryos. Wild-type zebrafish of the AB strain were maintained at 28 °C on a 14-h light/10-h dark cycle at the Department of Biology, Università degli Studi di Milano, according to ref. 49. Embryos were collected by natural spawning, staged and raised at 28 °C in fish water (Instant Ocean, 0.1% methylene blue, vol/vol) in Petri dishes.

htt morpholino. htt morpholino (Gene Tools) was designed to specifically target the zebrafish htt translation initiation codon (htt ATG MO, ATTTTAACA GAAGCTGTGATG)[27]. Injections were carried out on 1–2 cell-stage embryos (Eppendorf FemtoJet Micromanipulator 5171); the dye tracer, rhodamine dextran, was co-injected. A standard control morpholino oligonucleotide specific for human β-thalassemia was used.

Zebrafish histology and brain ventricle imaging. Embryos were anaesthetized in 0.1 mg ml^{-1} tricaine (Sigma) in embryo medium. Hindbrain ventricle microinjection was performed with 2–10 nl of dextran conjugated to rhodamine (5% in 0.2 mol l^{-1} KCl, vol/vol, Sigma). For histological sections, morphant and control embryos were fixed in Bouin's solution or 4% paraformaldehyde (vol/vol), dehydrated, paraffin embedded and sectioned (6–8 μm). The images were acquired with a Leica DM6000 B microscope equipped with LAS Leica imaging software (Leica).

Mouse tissues. We analyzed total brain tissues from mice (two mice per genotype), aged 1.75 months, with the conditional *Hdh* mutation, *Nestin-cre/+; Hdh*$^{loxP/-}$.

DNA transfections. *Hdh*$^{ex4-5}$ ES cells were plated at a density of 1–1.5 × 10^4 cells per cm^2. After 24 h, cells were transfected with different expression vectors (4 μg) and Lipofectamine 2000 (Invitrogen). Cells were selected with puromycin (2 μg ml^{-1}) 24 h after lipofection for 15 d. Cells were lysed and reverse-transcription PCR, western blot and immunofluorescence were performed to determine the presence of the transgene. The same protocol was used for transient transfection experiments during monolayer protocol (day 2, 3 and 4).

Constructs. The N-terminal and C-terminal portion of htt were designed according to htt protein multialignment[2] and cloned in pCAG constructs: pCAG-*D. discoideum*-N569-HA, pCAG-*S. purpuratus*-N519-HA, pCAG-*C. intestinalis*-N409-HA, pCAG-*B. floridae*-N478-HA, pCAG-*D. rerio*-N517-HA, pCAG-*M. musculus*-N548, pCAG-*M. musculus*-N548-HA, pCAG-*H. sapiens*-N652-15Q, pCAG-*M. musculus*-C-650-HA, pCAG-*D. melanogaster*-N548-HA. For full-length htt transfection, we used the 3xFLAG-7Q full-length mouse produced by S.Z. The Ncadherin cleavage–defective plasmid (*cdh2-GD-HA*) was created by site-directed mutagenesis as described previously[36].

siRNA transfection. 100 nM htt siRNA and scrambled siRNA from Dharmacon were transfected into R1 ES cells (*Hdh*$^{+/+}$) with the Amaxa mouse ES cell nucleofector kit (A-24 program). 100 pmol ADAM10 siRNA and scrambled siRNA from Invitrogen was transfected into *Hdh*$^{ex4-5}$ ES cells with Lipofectamine 2000. After 24 h, transfected cells were plated for neural differentiation[26]. During monolayer differentiation cells were transfected at day 2, 3 and 4 with 600 pmol htt siRNA and Lipofectamine 2000. RNA was collected from transfected cells 48 h post transfection and the analysis of *Hdh* mRNA knockdown was performed by real-time PCR.

Pharmacological treatments. On day 8 of neural differentiation, *Hdh*$^{ex4-5}$ and wild-type cells were incubated for 1 h with 34 μM TIMP1 (in phosphate-buffered saline, PBS).

GI254023X treatment of zebrafish embryos. We prepared 100 mM stock solution by dissolving GI254023X[25] in DMSO. Stock solutions were diluted in E3 medium (5 mM NaCl, 0.17 mM KCl, 0.33 mM $CaCl_2$, 0.33 mM $MgSO_4$) to final concentration of 40 μM. Embryos at 80% epiboly were dechorionated to allow access to the compound and were incubated in 2.5 ml compound dilutions or control medium (DMSO final concentration was 0.04%, vol/vol) in 12-well plates for 24 h. ADAM10 sequences analysis was performed by means of NCBI and Ensembl databases and related tools.

Immunofluorescence. Cells were fixed in 4% paraformaldehyde for 15 min at 20–23 °C. Cells were permeabilized in PBS with 0.5% Triton X-100 (vol/vol) and blocked with 5% fetal calf serum (vol/vol) for 1 h. Primary antibodies were diluted in blocking buffer and applied overnight at 4 °C. After three washes in PBS, appropriate secondary antibodies, conjugated to Alexa fluorophores 488 or 568 (Molecular Probes, Invitrogen) and diluted 1:500 in blocking solution, were applied for 1 h at 20–23 °C. Cells were incubated for 10 min with Hoechst 33258 (5 μg ml^{-1}, Molecular Probes, Invitrogen). Images were acquired with a Leica DMI 6000B microscope (equipped with LAS-AF imaging software) and processed with Adobe Photoshop and ImageJ (US National Institutes of Health) software.

Rosettes quantification. Rosettes were quantified in cell cultures on day 8 of neural differentiation after staining for Nestin. Ten images of random fields for each cell line were acquired. Each experiment was independently repeated at least three times. ImageJ analysis software was applied to calculate the area occupied by Nestin$^+$ cells as the total for normalization of each field. The shape of each rosette was outlined and the area occupied by Nestin staining was taken as area occupied by Nestin$^+$ cells inside rosettes. The remaining Nestin signal was taken as the area occupied by Nestin$^+$ cells outside rosettes. Data in graphs indicate the percentage of area occupied by Nestin$^+$ cells inside and outside of rosettes.

Protein lysates and western blot. Cells and mouse brain tissue were lysed in RIPA buffer (50 mM Tris-HCl pH 8, 150 mM NaCl, 0.1% SDS, 1% nonidet P40, 0.5% sodium deoxycholate, wt/vol) with 1 mM PMSF, 1 mM DTT, and protease inhibitor (Sigma). Lysates were cleared by centrifugation for 30 min at 12,000*g* at 4 °C. The resulting supernatant was collected. Protein concentration was determined with the BCA assay (Pierce) and 30–60 μg were loaded on a 10% SDS-PAGE gel. Separated proteins were transferred onto a nitrocellulose membrane, blocked with 5% nonfat dry milk (wt/vol, Biorad) in Tris-buffered saline (TBS) and 0.1% Tween-20 (vol/vol), and incubated with primary antibodies at 20–23 °C for 2 h. After washing, filters were incubated for 1 h at 20–23 °C with a secondary antibody (peroxidase conjugate, Biorad, 1:3,000) and then washed three times with TBS and 0.1% Tween-20. The SuperSignal West Pico Chemiluminescent Substrate (Pierce) was used to visualize immunoreactive bands by exposure to Amersham ECL Hyperfilm (GE Healthcare).

Co-immunoprecipitation. For ADAM10 and htt immunoprecipitation, we prepared total protein extracts as previously described. We precleared 500 μg protein homogenate in a final volume of 300 μl with 1/10 volume of Protein G–sepharose beads (GE HealthCare) after rocking for 1 h at 4 °C. The precleared supernatants were incubated with 3 μg of antibody to ADAM10 (Abcam) or 5 μg of antibody to htt (Mab2166 Millipore) overnight at 4 °C. Protein G–sepharose

doi:10.1038/nn.3080

beads were added and incubation was continued for 3 h, at 4 °C, with shaking. The beads were washed three times with RIPA buffer. Sample buffer for SDS-PAGE was added, and the mixture was heated for 10 min. Beads were collected by centrifugation and a volume of supernatant was applied onto 10% SDS-PAGE. ADAM10 immunocomplex precipitation was revealed by monoclonal antibody to SAP97 (Enzo Life Sciences) and huntingtin immunocomplex precipitation was revealed by polyclonal antibody to ADAM10 (kindly provided by P. Saftig).

***In situ* hybridization and immunohistochemistry of zebrafish embryos.** Whole-mount *in situ* hybridization was carried out as described previously[50] on embryos fixed for 2 h in 4% paraformaldehyde in PBS, then rinsed with PBS-Tween, dehydrated in 100% methanol and stored at −20 °C until processed[51]. For ZO-1 immunohistochemistry, embryos were exposed to ZO-1 primary antibody (Zymed, 1:300), then treated with a biotinylated secondary antibody (Vector Laboratories). Digital images of all embryos were captured using a digital camera (Leica).

Zebrafish western blots. Ncadherin western blots were prepared with 30 dechorionated and deyolked embryos (24 hpf) lysed in 100 µl of RIPA buffer with 1 mM PMSF and protease inhibitors. Samples were sonicated four times with 15-s pulses (microprobe at 40–50% output and 70% duty cycle). SDS sample buffer was added to the samples, and proteins were separated on a 10% SDS-PAGE gel and transferred to a nitrocellulose membrane at 90 mA overnight. The membrane was blocked and incubated overnight as described above with an antibody to the prodomain of zebrafish Ncadherin (kindly provided by E. Ruthazer), diluted 1:5,000. After four 15-min washes in blocking solution, the membrane was incubated for 1 h with secondary antibody to rabbit (peroxidase conjugate, Bio-Rad, 1:5,000) prepared in 5% nonfat dry milk in TBS and 0.3% Tween-20. The membrane was then washed three times in TBS and 0.3% Tween-20 before detection by chemiluminescence with SuperSignal West Femto Substrate (Pierce).

Antibodies. The antibodies and dilutions used for immunofluorescence or immunohistochemistry (IHC) and western blotting were: monoclonal antibody to HA (Covance; immunofluorescence, 1:500; western blotting, 1:1,000), monoclonal antibody to huntingtin (Mab2166, Millipore; immunofluorescence, 1:800; western blotting, 1:2,000), monoclonal antibody to MAP2 (Becton Dickinson; immunofluorescence, 1:1,000), monoclonal antibody to Ncadherin (Becton Dickinson; immunofluorescence, 1:1,000; western blotting, 1:4,000), monoclonal antibody to Nestin (Millipore; immunofluorescence, 1:200), monoclonal antibody to α-tubulin (Sigma; western blotting, 1:3,000), polyclonal antibody to ADAM10 (kindly provided by P. Saftig; western blotting, 1:1,000); polyclonal antibody to Ncadherin (zebrafish) (kindly provided from E. Ruthazer), monoclonal antibody to SAP97 (Enzo Life Sciences; western blotting, 1:1,000); polyclonal antibody to GFAP (Dako; immunofluorescence, 1:1,000), polyclonal antibody to ZO1 (Zymed; IHC, 1:50), polyclonal antibody to GAP43 (Chemicon; immunofluorescence, 1:500), polyclonal antobody to β-3 tubulin (Covance; immunofluorescence, 1:1,000) and polyclonal antibody to Sox1 (Santa Cruz; immunofluorescence, 1:100).

RNA extraction and reverse transcription. Total RNA was extracted with the Trizol reagent (Invitrogen). Total RNA concentration was measured with a NanoDrop 1000 Spectrophotometer (Thermo Scientific). For mRNA detection, 1,000 ng of total RNA was reverse-transcribed to single-stranded cDNA with Superscript reverse transcriptase (Invitrogen) and 250 ng of random primers.

Real-time PCR. We used an iCycler Thermal Cycler with a Multicolor Real-time PCR Detection System (Bio-Rad). All reactions were performed in a total volume of 25 µl with 5 µl of cDNA, 20 µl iQTM SYBR Green Supermix-Bio-Rad, and 0.2 µM each of forward and reverse primers. The amplification consisted of 95 °C for 3 min, and 45 cycles of 30 s at 95 °C, 30 s at 60 °C and 30 s at 72 °C. Fluorescence was quantified during the annealing step and product formation was confirmed by melting curve analysis (55–94 °C). We used primers for *Adam10* (forward, GGAAGCTTTAGTCATGGGTCTG; reverse, CTCCTTCCTCTACTCCAGTCATT, annealing 60 °C), *Cdh2* (forward, AACACAGCCACAGCCGTCATC; reverse, CTTTGTCCGTGACAG TTAGGTTGT, annealing 60 °C), *Sap97* (also known as *Dlg1*; forward, GT GTGCCGCCTTCCTGATTCTG; reverse, CCCGCTCTATGGAACTTCTGAG) and *Hdh* (forward, CGCTATGGAACTGTTTCTGCTGTG; reverse, CTGTAGC CTTGGAAGATTAGAATCCATCT, annealing 60 °C).

Apo-tox Glo triplex Assay. Cells were seeded in triplicate in a 96-well plate, at 5×10^3 cells per well. After an 8-h incubation at 37 °C, cells received 100 µl of freshly prepared GMEM+LIF without serum. At 24 h after plating, 20 µl of viability reagent was added to all wells. After 1 h of incubation at 37 °C, fluorescence was measured at 400Ex/505Em with a Synergy HT multi-detection microplate reader (BioTek). Caspase-Glo 3/7 Reagent (100 µl) was added to all wells. After 30 min of incubation at 20–23 °C, luminescence was recorded with a Veritas-Microplate Luminometer (Turner Biosystems). Each experiment was independently repeated at least three times. Results are presented as the ratio of luminescence/fluorescence recorded for each cell line.

Statistical analyses. Two-tailed unpaired *t* test or one-way ANOVA and Bonferroni *post hoc* test were used. *P* values, s.d., s.e.m. and mean values were calculated using GraphPad Prism version 4.0.

49. Westerfield, M. *The Zebrafish Book* (University of Oregon Press, 1993).
50. Thisse, C., Thisse, B., Schilling, T.F. & Postlethwait, J.H. Structure of the zebrafish snail1 gene and its expression in wild-type, spadetail and no tail mutant embryos. *Development* **119**, 1203–1215 (1993).
51. Jowett, T. & Lettice, L. Whole-mount *in situ* hybridizations on zebrafish embryos using a mixture of digoxigenin- and fluorescein-labeled probes. *Trends Genet.* **10**, 73–74 (1994).